Electronic Supplementary Material (ESI) for Journal of Materials Chemistry A.

Supporting information

Electrochemical Performance of $M(dca)_2pyz$ (M= Fe, Co, and Ni) MOFs as Sustainable Anodes in Lithium-Ion Batteries

Isabel Ciria-Ramos[a,b], Alberto García-Fernández[c], Álvaro Mayoral[a], Alodia Orera[a], Emilio J. Juarez-Perez[a,d,*] and Marta Haro[a,b,*]

[a] Instituto de Nanociencia y Materiales de Aragón (INMA), CSIC-Universidad de Zaragoza, Zaragoza, 50009, Spain

[b] Departamento de Química Física, Facultad de Ciencias, Universidad de Zaragoza, Plaza San Francisco, Zaragoza, 50009, Spain

[c] Division of Applied Physical Chemistry, Department of Chemistry, KTH Royal Institute of Technology, SE-100 44 Stockholm, Sweden

[d] Aragonese Foundation for Research and Development (ARAID). Government of Aragon, Zaragoza, 50018, Spain

[*]mharo@unizar.es; ejjuarezperez@unizar.es

Table of contents

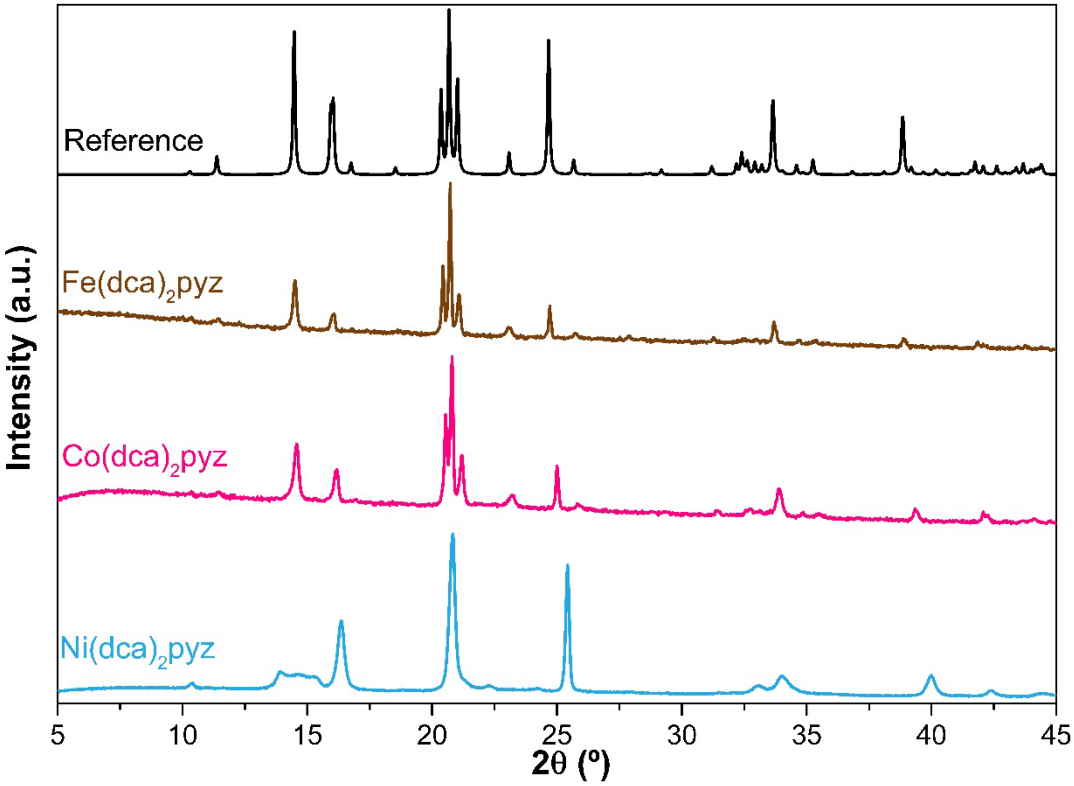

Figure S1. Room temperature PXRD patterns for the as-prepared $M(dca)_2pyz$ (M= Fe, Co or Ni) compounds and the simulated one based on the single crystal data obtained at room temperature.[1]

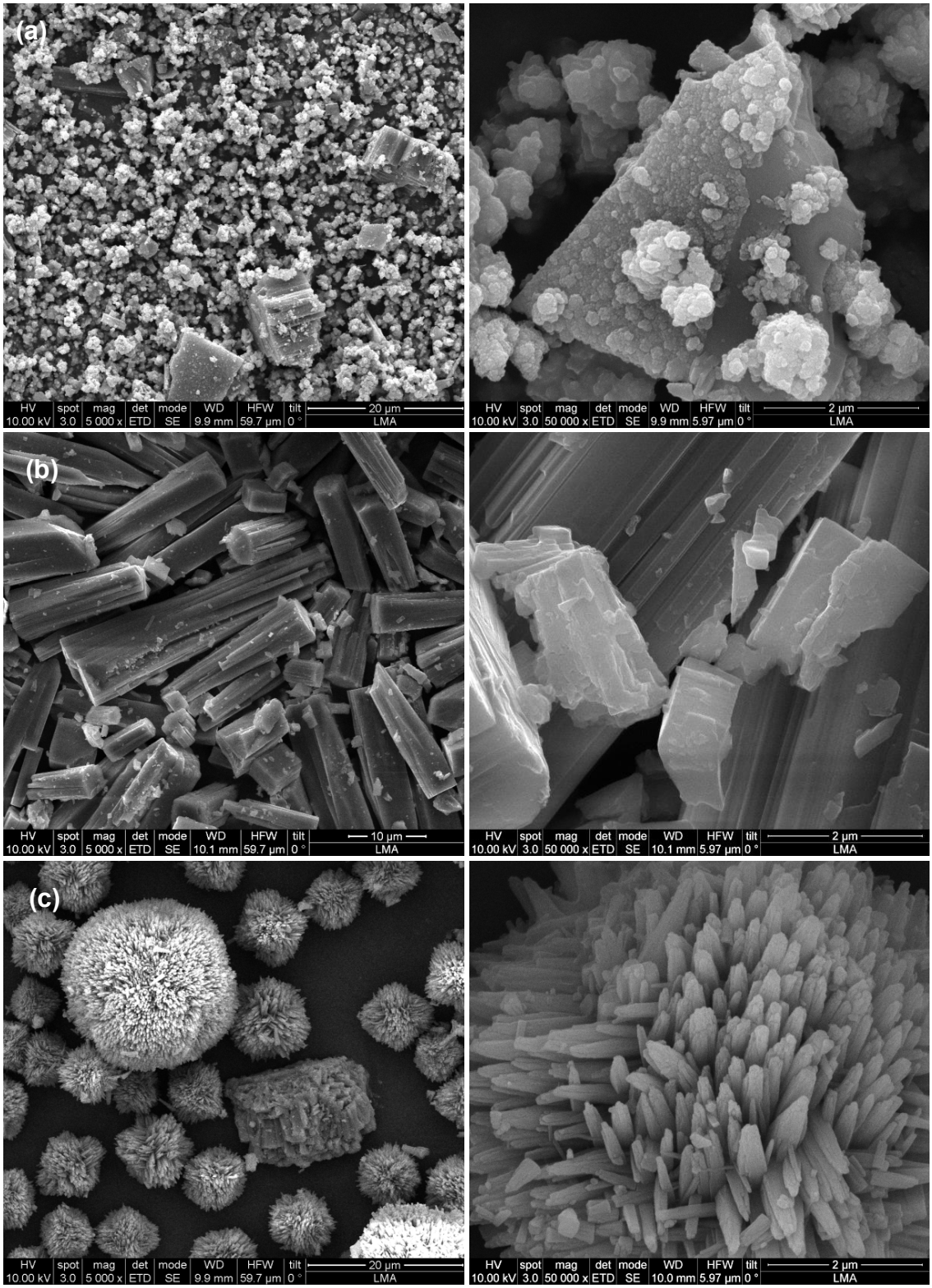

Figure S2. SEM images of **a)** $Fe(dca)_2pyz$, **b)** $Co(dca)_2pyz$ and **c)** Ni $(dca)_2pyz$.

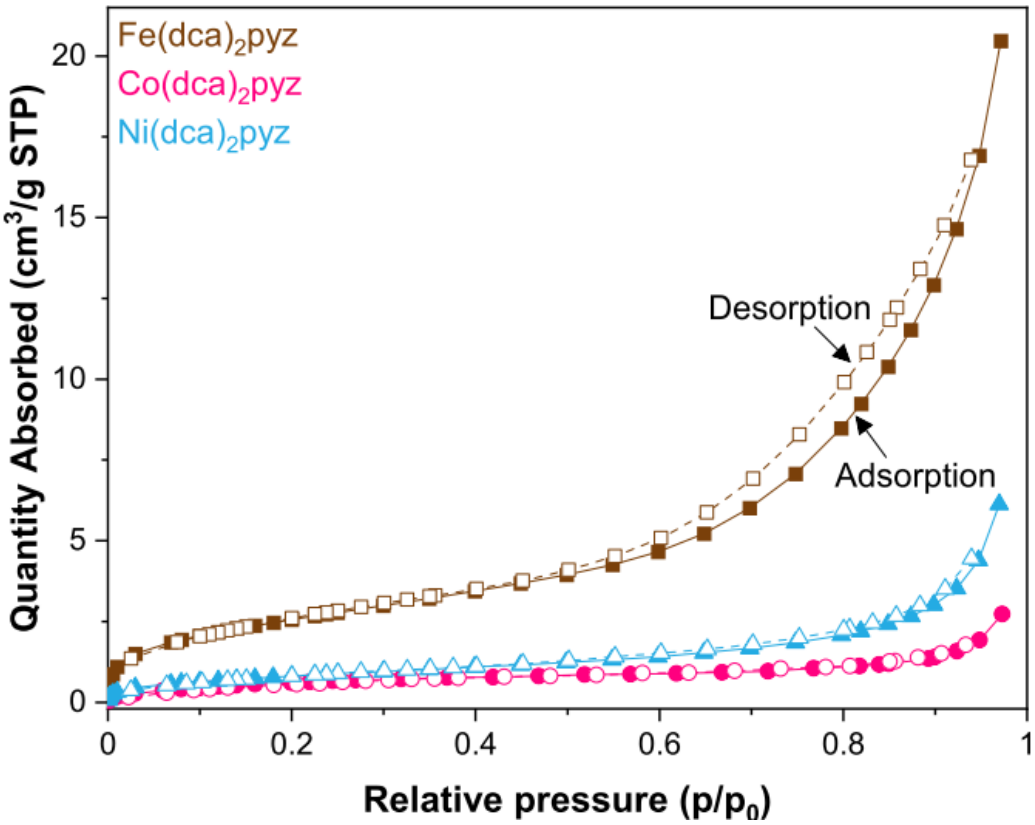

Figure S3. N_2 adsorption isotherms of $Ni(dca)_2pyz$, $Co(dca)_2pyz$, and $Fe(dca)_2pyz$.

N_2 adsorption isotherms at 77 K in a Micromeritics TriStar 3000 established the specific surface area and pore volume distribution for samples previously out-gassed during 10 h at 200 ºC and 20 Pa.

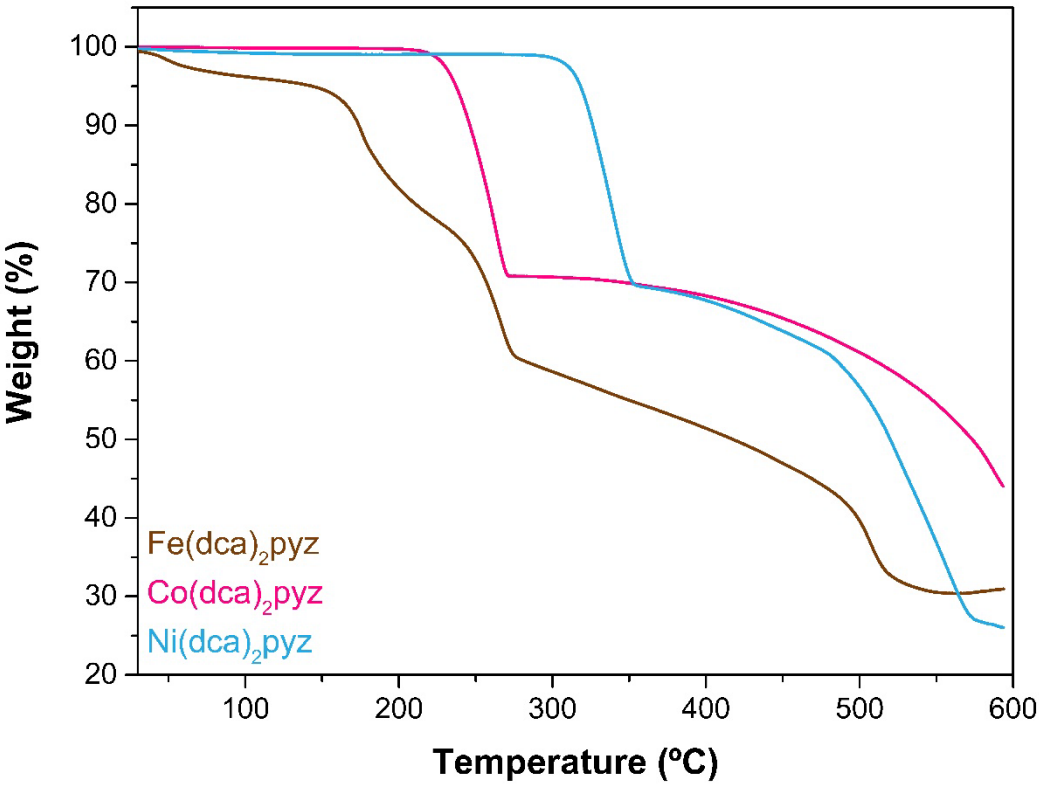

Figure S4. TGA curves of $Fe(dca)_2pyz$ (brown), $Co(dca)_2pyz$ (pink) and $Ni(dca)_2pyz$ (blue).

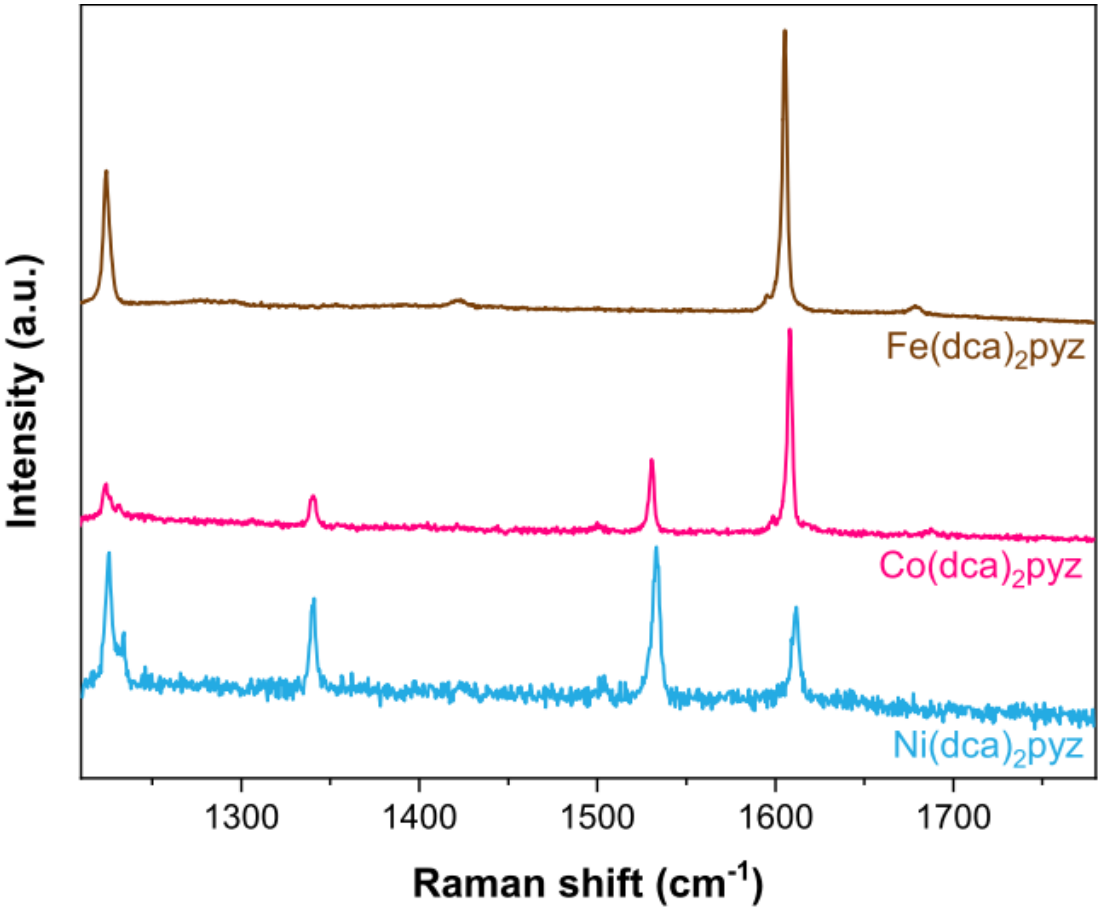

Figure S5. Raman spectra of the three MOFs in the region of D and G bands. The three MOFs show the two fundamental vibrations of A_g symmetry at ~1240 cm^{-1} and ~1600 cm^{-1}, assigned to the C-H in plane deformation (δ_{9a}) and the ring stretching (ν_{8a}), respectively.[2] The blue-shift observed for this last peak indicates stronger interaction between the N two electrons and the M, being Fe < Co < Ni. Also, two more bands appear in $Co(dca)_2pyz$ and $Ni(dca)_2pyz$, at ~1340 cm^{-1} and ~1535 cm^{-1} plausibly attributed to C-H in plane deformation (δ_3) and the ring stretching (ν_{8b}) corresponding to B_{3g} symmetry. The enhancement of the B_{3g} symmetry modes, particularly 8b fundamental, is attributed to the vibronic coupling between the D_0 and D_1 states of the radical anion,[3] being more noticeable this effect for $Ni(dca)_2pyz$, in which the intensity of 8b band is higher than 8a band. These effects suggest that the interaction between Ni-pyz is stronger than Co-pyz and Fe-pyz.

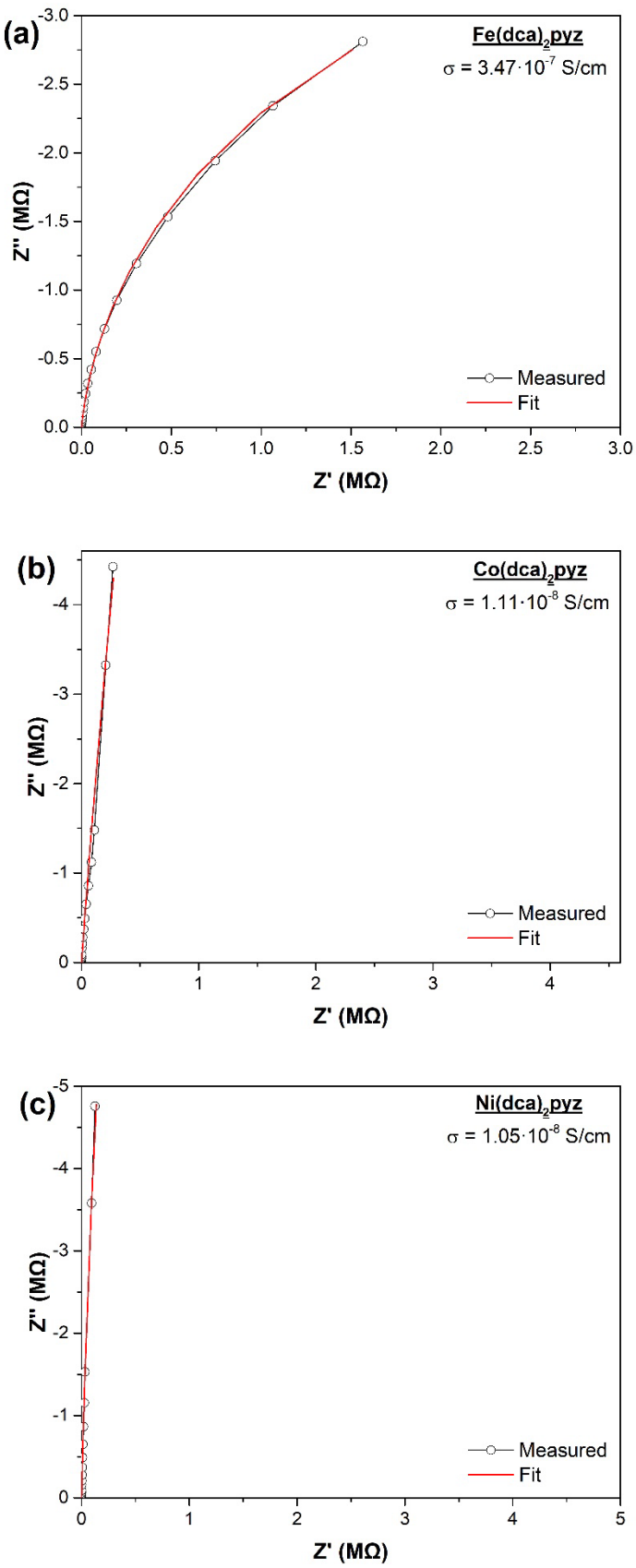

Figure S6. EIS spectra obtained at a pressure of 226 MPa and applying a voltage of 1 V and the fit of the powders **a)** $Fe(dca)_2pyz$, **b)** $Co(dca)_2pyz$ and **c)** Ni $(dca)_2pyz$.

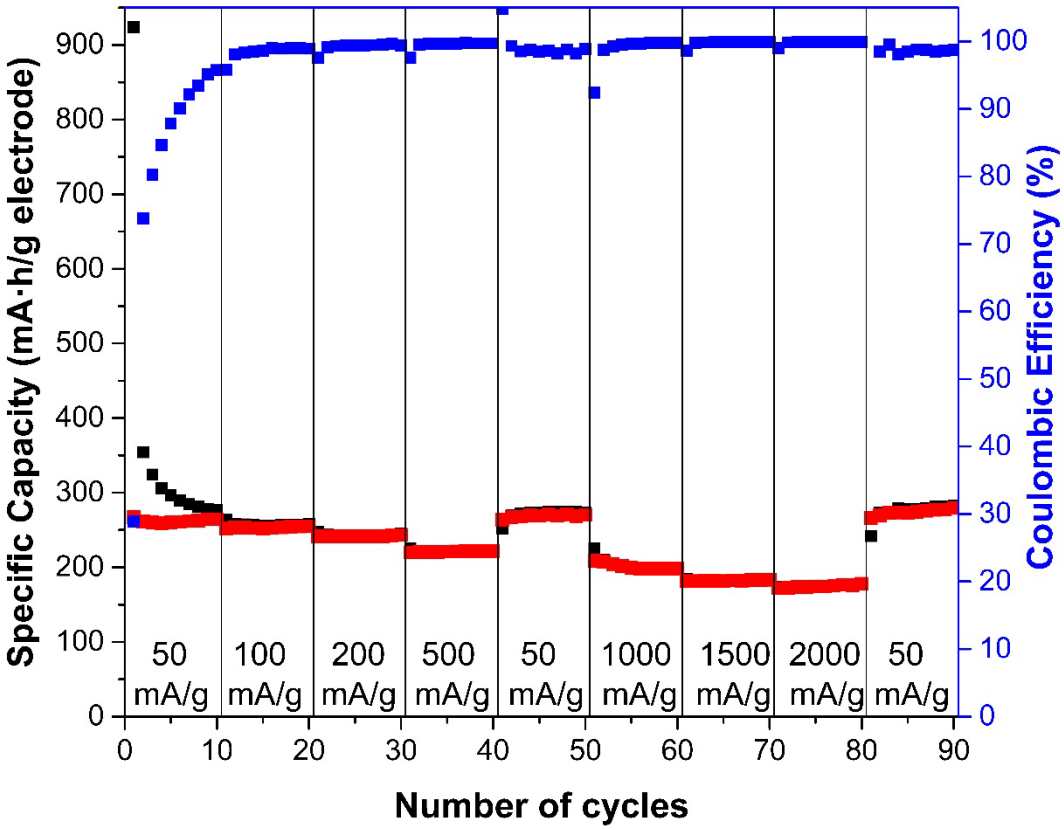

Figure S7. Lithiation (black) and delithiation (red) specific capacity and Coulombic Efficiency (blue) of an electrode composed of 95 % in weight of carbon black and 5 % in weight of polyvinylidene fluoride (the binder) at different rates. The current applied considers the mass of carbon black in the electrode whereas the specific capacity uses the mass of the complete electrode (it also considers the binder mass).

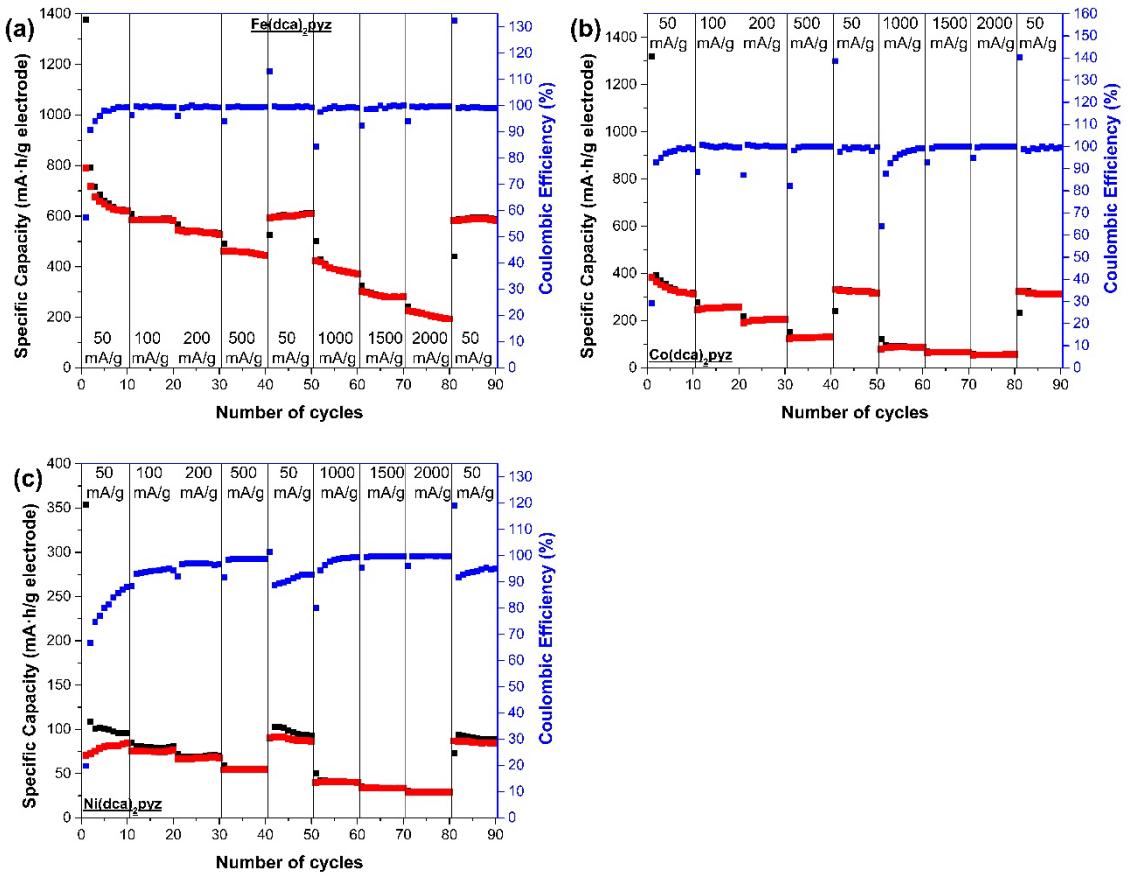

Figure S8. Lithiation (black) and delithiation (red) specific capacity and Coulombic Efficiency (blue) of the electrodes containing **a)** $Fe(dca)_2pyz$, **b)** $Co(dca)_2pyz$ and **c)** $Ni(dca)_2pyz$. The current applied considers the mass of the MOF in the electrode whereas the specific capacity uses the mass of the complete electrode (it also considers mass of the carbon additive and the binder).

Coulombic Efficiencies (CE) in the first cycle of Fe, Co, Ni electrodes are 57% (1376/789 $mAhg^{-1}$), 29 % (1055/307 $mAhg^{-1}$), and 20 % (354/70 $mAhg^{-1}$), respectively. This low CE is a consequence of the formation of the solid electrolyte interface (SEI) by electrolyte-electrode surface reaction. In the subsequent lithiation/delithiation cycles the Coulombic Efficiency increases for the $Fe(dca)_2pyz$ and $Co(dca)_2pyz$ electrodes until approaching a value of 100 %. In contrast, Ni electrode presents lower CE values at low rates (~93 % at 50 mA/g) which increase with the applied current until they reach values higher than 99 % at 1000 mA/g.

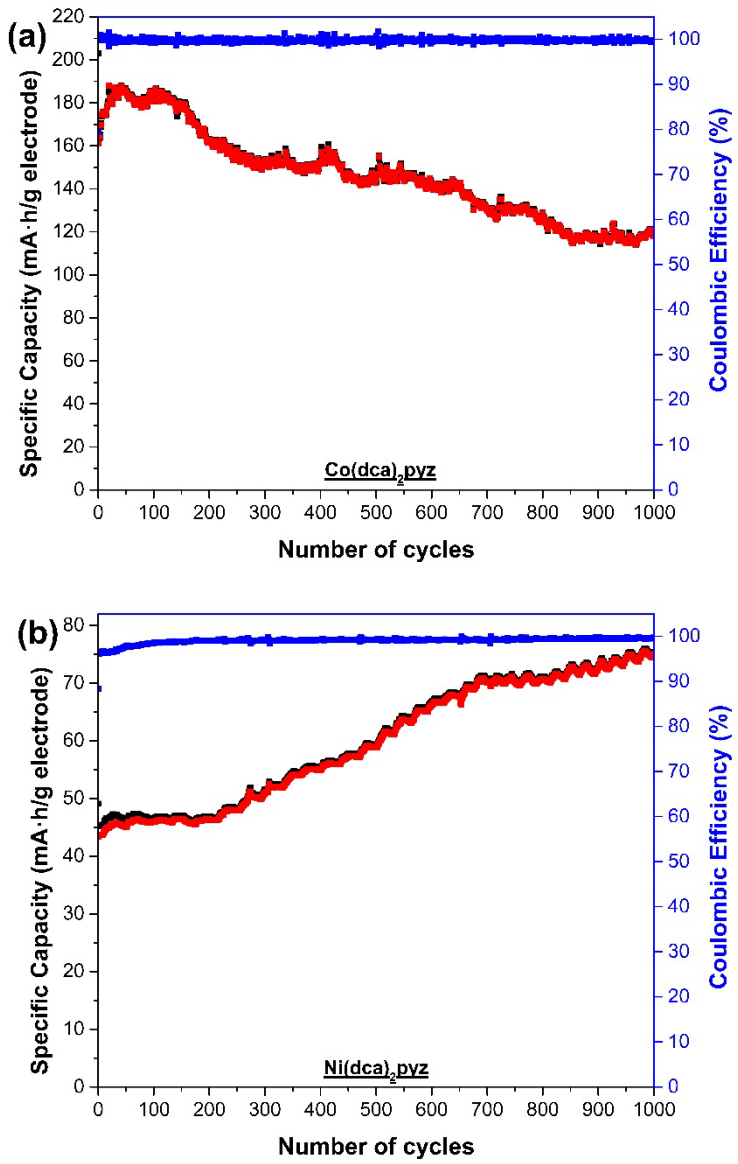

Figure S9. Rate performance at 200 mA/g of the electrodes containing **a)** $Co(dca)_2pyz$ and **b)** $Ni(dca)_2pyz$ showing the lithiation (black) and delithiation (red) specific capacity and the Coulombic Efficiency (blue). 10 conditioning cycles at 50 mA/g have been done before these cycles. The current applied considers the mass of the MOF in the electrode whereas the specific capacity uses the mass of the complete electrode (it also considers mass of the carbon additive and the binder).

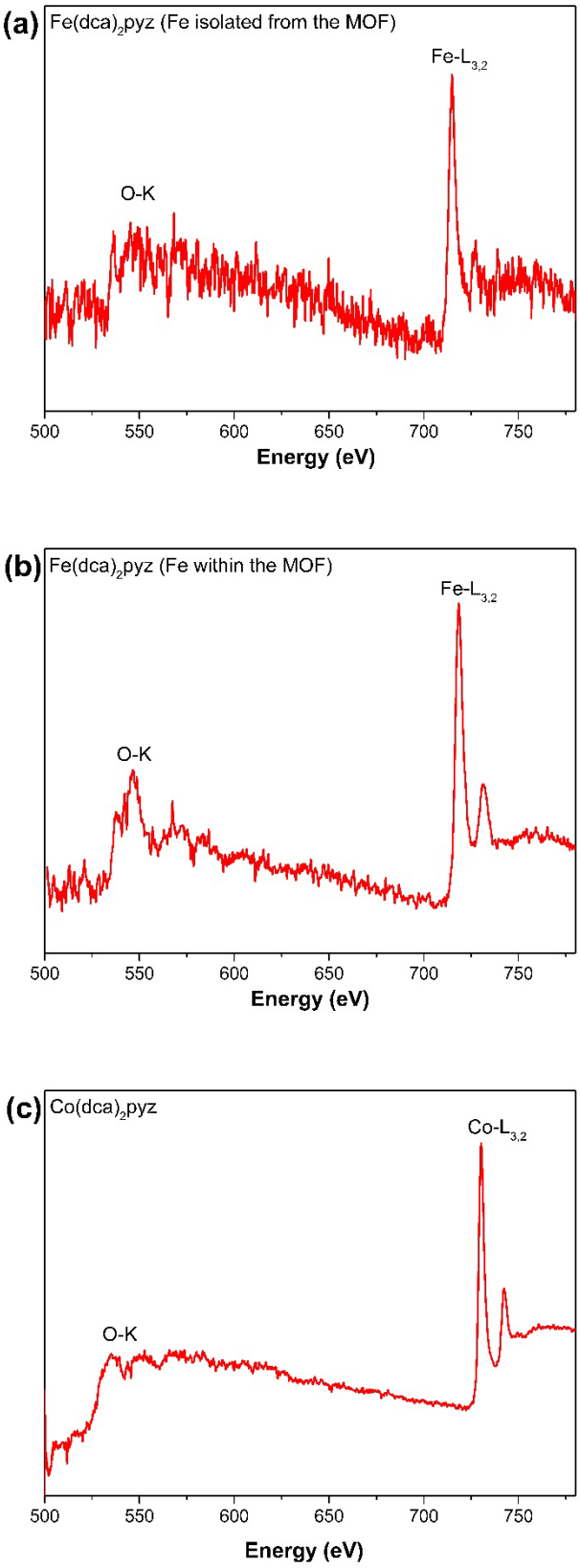

Figure S10. EEL spectra of **a)** isolated Fe from $Fe(dca)_2pyz$, **b)** Fe within the MOF $Fe(dca)_2pyz$ and **c)** $Co(dca)_2pyz$.

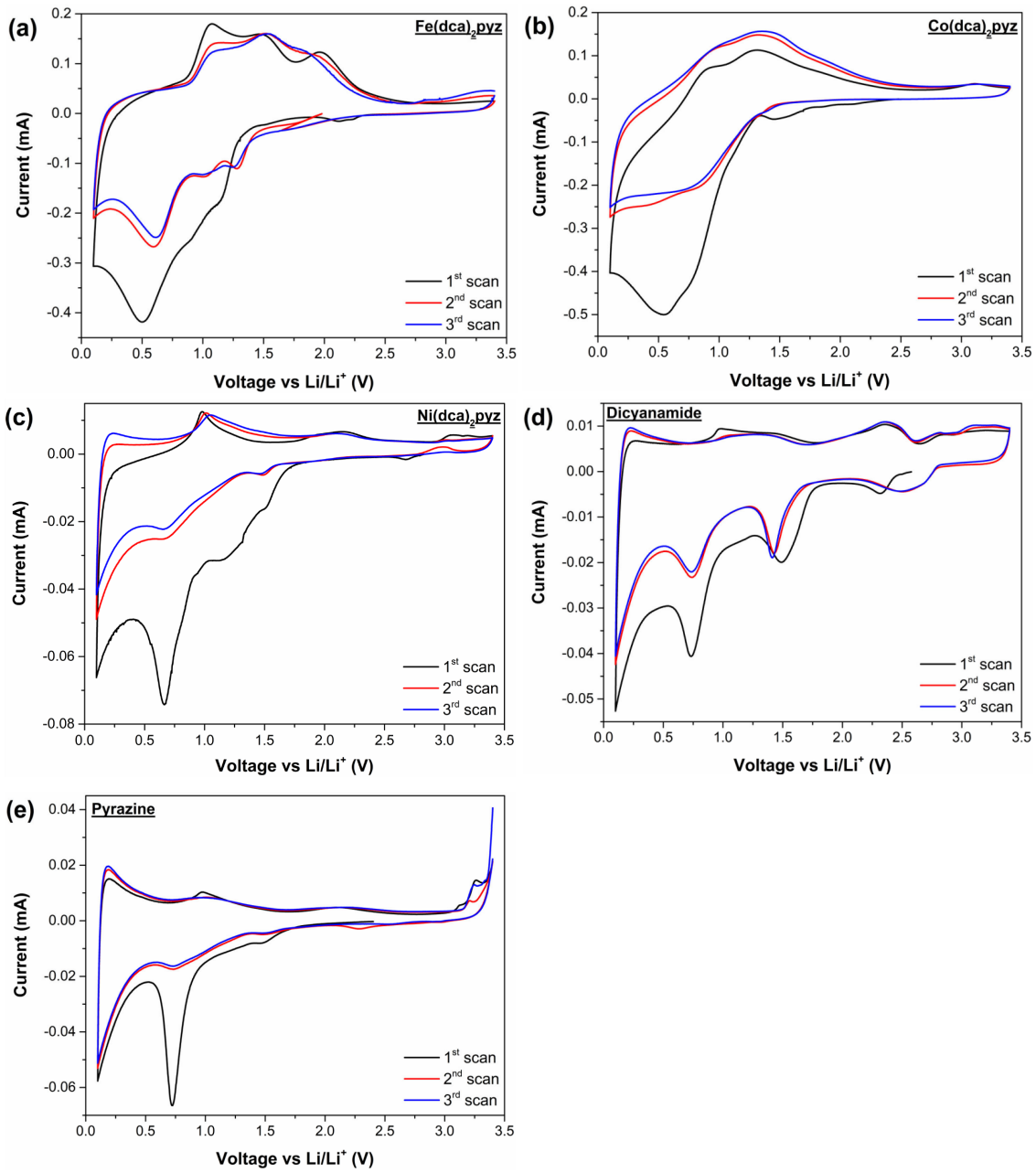

Figure S11. First three CVs obtained at a scan rate of 0.1 mV/s of the compounds **a)** $Fe(dca)_2pyz$, **b)** $Co(dca)_2pyz$ and **c)** $Ni(dca)_2pyz$, and their ligands **d)** dicyanamide and **e)** pyrazine.

Both ligands present two cathodic peaks at 0.75 V and 0.1 V vs Li/Li^+. Moreover, dca shows an additional cathodic peak at ~1.5V vs Li/Li^+, assigned to the interaction of Li^+ with dca central N, the preferred position for the alkaline metal in dicyanamide salts.[4] The peak at 0.75V is allocated to SEI formation and it diminishes rapidly after the first cycle, being more notable in the pyz ligand. Conversely, in dca, the peak remains intense and reproducible in the second and third cycles, suggesting an additional redox process around 0.7 V vs Li/Li^+. This behavior, prominently observed in dca and minimally in pyz, likely relates to the interaction of Li^+ ions with their terminal N. The last peak at 0.1V

indicates the stabilization of Li^+ ions with delocalized π electrons from double/triple bonds in dca, and from the aromatic ring in pyz. Despite the observation of these peaks in the CV, the specific capacities (Figure S12) remain low, which means that polymerization within coordinated polymers through TM nodes improves the storage capacity of Li^+ ions.

The Ni-MOF shows after the SEI formation in the first cycle, a main peak at 0.1 V where Li^+ ions intercalate and interact with π electrons from the ligands. In the case of Fe-MOF the largest peak appears at ~0.5 V, and two smaller peaks at ~1 V and ~1.5 V, related to the reduction of Fe nodes and interaction between Li and the N of the ligands. Co-MOF shows a broad CV peak below ~1.3 V, instead of well-defined peaks, suggesting that the limitation arises from kinetic constraints. The significantly lower electrical conductivity of Co-MOF, compared to Fe-MOF, may impede charge compensation and lead to electrostatic repulsions.[5]

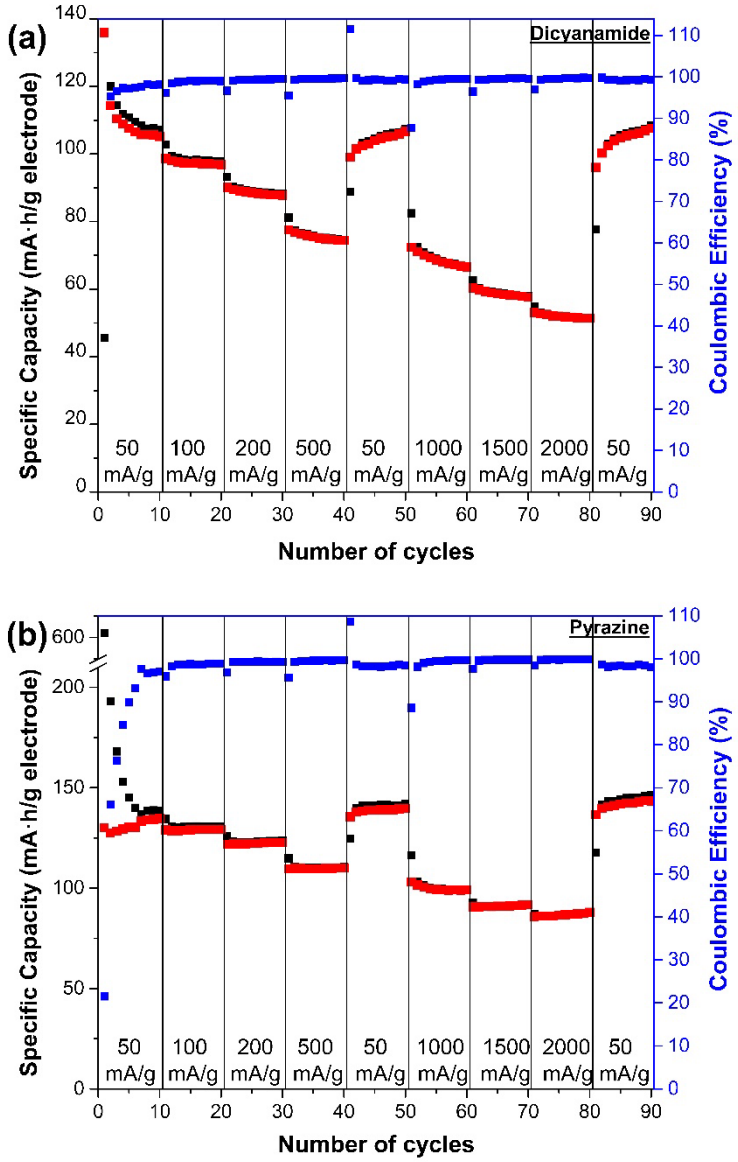

Figure S12. Lithiation (black) and delithiation (red) specific capacity and Coulombic Efficiency (blue) of the ligands **a)** dicyanamide and **b)** pyrazine. The current applied considers the mass of the ligand in the electrode whereas the specific capacity uses the mass of the complete electrode (it also considers mass of the carbon additive and the binder).

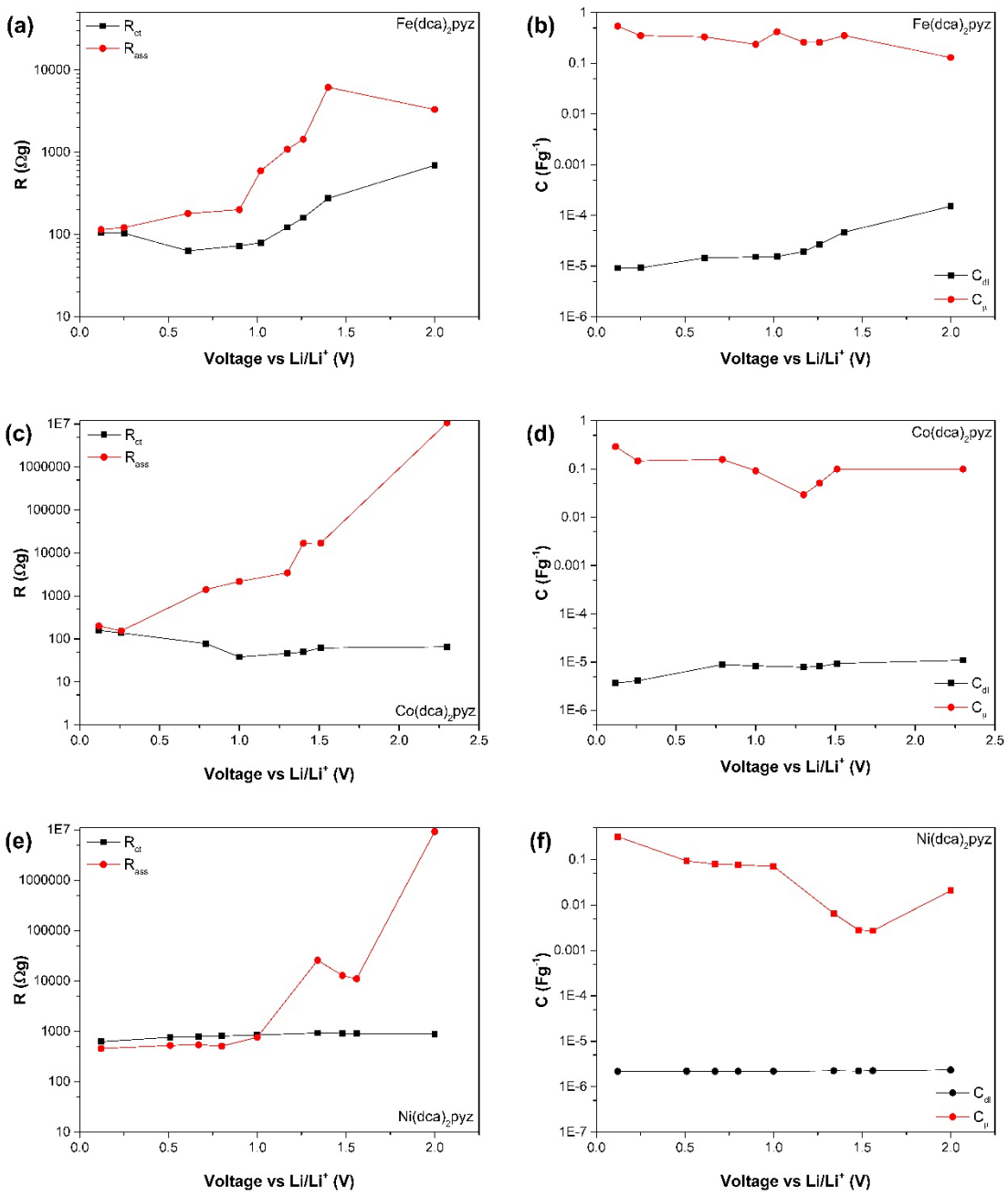

Figure S13. Calculated resistances (**a**), **c)** and **e)**) and capacitances (**b**), **d)** and **f)**) fitted for the equivalent circuit model illustrated in Figure 7. The resistances obtained in the Fe-MOF range between 10 and 10^4 Ωg. Co-MOF and Ni-MOF show resistances up to 10^7Ωg. Although at low voltages when Li^+ ions are intercalated the resistance in both MOFs decreases, the chemical capacitances remain practically an order of magnitude below that of Fe-MOF. This indicates that not only kinetic restrains are responsible of the lower capacities registered during charging/discharging cycles, but also thermodynamic ones, probably due to the strength of the M-N binding energy.

Table S1. Comparison of Li^+ storage capacity of our materials with reported literature of TMNs.

Active material	Active material: Carbon additive: PVDF	Voltage range (V)	Rate (mA/g)	Reversible capacity (mAh/g)	Number of cycles	Reference
Fe_2N@CNFs	80:10:10	3-?	100	100	60	6
Co_2N@CNFs	80:10:10	3-?	100	563	50	
Fe_3N@C	80:10:10	2-0.01	100	358	500	7
Fe_2N@C in CSHN	70:20:10	3-?	200	~600	200	8
			5000	~600	1000	
Fe_2N/rGO	85:5:10	3-0.005	100	578	500	9
Fe_2N/rGO	80:10:10	3-0.01	200	378	200	10
			500	368	200	
Fe_3N/rGO	80:10:10	3-0.01	200	615	200	
			500	513	200	
Fe_2N@C-rGO	80:10:10	3-0.01	100	760	100	11
FeN/N-rGO	80:10:10	3-0.01	50	698	50	12
			100	~560	100	
CoN/N-rGO	80:10:10	3-0.01	50	730	80	
FeCoN/N-rGO	80:10:10	3-0.01	100	520	60	
NiN/N-rGO	80:10:10	3-0.01	50	667	80	

$(Ni/Co)_3N$ MC@HC	70:20:10	3-0.01	200	440	130	[13]
			500	170	130	
om-CoN	80:10:10	3-0.01	1000	710	350	[14]
			2000	300	2000	
$NiCo_2N$@C-NCNT	70:20:10	3-0.01	200	750.6	500	[15]
			2000	569.1	500	
Porous CoN	70:15:15	3-0.005	250	660	60	[16]
			1000	470	60	
CoN	70:15:15	3-0.005	60	956	60	[17]
Ni_3N	84:8:8	3-0.001	1 Li in 5 hours	~530	10	[18]
			1 Li in 1 hour	~430	10	
$NiCo_2N$	70:20:10	3-0.01	1000	1244.5	400	[19]
Ni_3N–Co_3N@CNT	70:20:10	3-?	400	553.3	600	[20]
Co_3N@CNT	70:20:10	3-?	400	249.8	600	
Ni_3N@CNT	70:20:10	3-?	400	327.4	600	
$Fe(dca)_2pyz$	80:15:5	3-0.1	200	649.1	450	This work
$Co(dca)_2pyz$	80:15:5	3-0.1	200	184.5	450	
		3-0.1	200	147.4	1000	
$Ni(dca)_2pyz$	80:15:5	3-0.1	200	71.5	450	
		3-0.1	200	94.2	1000	

CNFs =Carbon Nanosheet Frameworks
C = Carbon-constraint
CSHN = Core−Shell Hybrid Fibers
rGO = reduced Graphene Oxide
MC@HC = Multi-Core@Hollow Carbon shell
om = ordered mesoporous
NCNT = Nitrogen-doped Carbon NanoTubes
CNT = Carbon NanoTubes

Table S2. Comparison of Li^+ storage capacity of our materials with reported literature of Fe, Co and Ni-MOFs.

Active material	Active material: Carbon additive: PVDF	Voltage range (V)	Rate (mA/g)	Reversible capacity (mAh/g)	Number of cycles	Reference
Fe(OH)(BDC)	70:20:10	3-0.01	100	310	100	21
Fe(1,4-Dicarboxybenzene)	70:20:10	3-0.01	500	~930	200	22
$[Fe_3O(BDC)_3(H_2O)_2(NO_3)]_n$	60:30:10	3-0.005	60	744.5	400	23
PCN-600	60:30:10	3-0	400	~1000*	300	24
mFeP-NM	60:30:10	3-0.001	200	300	350	25
$Co_2(NDC)_2(DMF)_2$	55:35:10	3-0.01	200	623.6	100	26
$[Co_2(py\text{-}TTF\text{-}py)_2(BDC)_2]\cdot 2DMF\cdot H_2O$	60:30:10	3-0.01	200	1186.6	287	27
			1000	1043.8	234	
			5000	758.6	313	
$[Co_2(py\text{-}TTF\text{-}py)_2(BPDC)_2]\cdot 3DMF\cdot 3H_2O$	60:30:10	3-0.01	200	1054.6	174	
$Co_2(OH)_2BDC$	70:25:5	3-0.01	100	948	100	28
$Co(HNA)_2(H_2O)_4$	70:20:10	3-0.01	100	455	60	29
$[Co(HNA)]_n$	70:20:10	3-0.01	100	618	100	
$Ni(HNA)_2(H_2O)_4$	70:20:10	3-0.01	100	411	60	
$[Ni(HNA)]_n$	70:20:10	3-0.01	100	610	100	
$Ni(4,4'\text{-bpy})(tfbdc)(H_2O)_2$	60:30:10	3-0.01	50	406	50	30
$Ni_3(HITP)_2$	70:20:10	3-0.01	1000	712	200	31
			2000	~501	500	
			5000	362	500	
$Fe(dca)_2pyz$	80:15:5	3-0.1	200	649.1	450	This work
$Co(dca)_2pyz$	80:15:5	3-0.1	200	184.5	450	
		3-0.1	200	147.4	1000	
$Ni(dca)_2pyz$	80:15:5	3-0.1	200	71.5	450	
		3-0.1	200	94.2	1000	

PCN-600 = iron porphyrin-based MOF
BDC = 1,4-benzenedicarboxylate
mFeP-NM = mesoporous ferric phytate nanomeshes
DMF = N,N -dimethylformamide
NDC = 1,4-naphthalene dicarboxylate
H_2BDC = terephthalic acid

py-TTF-py = 2,6-bis(4′-pyridyl)tetrathiafulvalene

H_2NA = 5-hydroxynicotinic acid

H_2BPDC = biphenyl-4,4′-dicarboxylic acid

4,4′-bpy = 4,4′-bipyridine

H_2tfbdc = tetrafluoroterephthalic acid

HITP = 2,3,6,7,10,11-hexaaminotriphenylene

*The mass of the conductive additive is considered to calculate the specific capacity.

References

1 P. Jensen, S. R. Batten, B. Moubaraki and K. S. Murray, *J. Solid State Chem.*, 2001, **159**, 352–361.

2 Q. J. Huang, J. L. Yao, B. W. Mao, R. A. Gu and Z. Q. Tian, *Chem. Phys. Lett.*, 1997, **271**, 101–106.

3 J. F. Arenas, M. S. Woolley, I. Ló Pez Tocó, J. C. Otero and J. I. Marcos, 2000, **112**, 7669–7683.

4 O. Reckeweg, F. J. Disalvo, A. Schulz, B. Blaschkowski, S. Jagiella and T. Schleid, *Zeitschrift fur Anorg. und Allg. Chemie*, 2014, **640**, 851–855.

5 P. Mao, H. Fan, C. Liu, G. Lan, W. Huang, Z. Li, H. Mahmoud, R. Zheng, Z. Wang, H. Sun and Y. Liu, *Sustain. Energy Fuels*, 2022, **6**, 4075–4084.

6 Y. Dong, Y. Li, H. Shi, J. Qin, S. Zheng, R. He and Z. S. Wu, *Carbon N. Y.*, 2020, **159**, 213–220.

7 H. Huang, S. Gao, A. M. Wu, K. Cheng, X. N. Li, X. X. Gao, J. J. Zhao, X. L. Dong and G. Z. Cao, *Nano Energy*, 2017, **31**, 74–83.

8 X. Li, C. Deng, H. Wang, J. Si, S. Zhang and B. Huang, *ACS Appl. Mater. Interfaces*, 2021, **13**, 7297–7307.

9 M. Idrees, A. S. Haidyrah, Ata-ur-Rehman, Q. Zhang, X. Li and S. M. Abbas, *J. Alloys Compd.*, 2021, **883**, 160824.

10 L. Tian, Y. Xie, J. Lu, T. Liu, Q. Hu, Y. Xiao, X. Zhu and X. Su, *J. Alloys Compd.*, 2022, **922**, 166208.

11 P. Yu, L. Wang, F. Sun, D. Zhao, C. Tian, L. Zhao, X. Liu, J. Wang and H. Fu, *Chem. - A Eur. J.*, 2015, **21**, 3249–3256.

12 L. Lai, J. Zhu, B. Li, Y. Zhen, Z. Shen, Q. Yan and J. Lin, *Electrochim. Acta*, 2014, **134**, 28–34.

13 B. K. Kang, Y. J. Choi, H. W. Choi, S. Bin Kwon, S. Kim, Y. J. Kim, J. S. Park, W. S. Yang, D. H. Yoon and W. H. Ryu, *Chem. Eng. J.*, 2021, **420**, 129630.

14 G. Jiang, H. Han, W. Zhuang, X. Xu, S. Kaskel, F. Xu and H. Wang, *J. Mater. Chem. A*, 2019, **7**, 17561–17569.

15 R. Zou, M. Xu, S. A. He, X. Han, R. Lin, Z. Cui, G. He, D. J. L. Brett, Z. X. Guo,

J. Hu and I. P. Parkin, *J. Mater. Chem. A*, 2018, **6**, 19853–19862.

16 B. Das, M. V. Reddy, G. V. S. Rao and B. V. R. Chowdari, *J. Mater. Chem.*, 2012, **22**, 17505–17510.

17 M. V. Reddy, G. Prithvi, K. P. Loh and B. V. R. Chowdari, *ACS Appl. Mater. Interfaces*, 2014, **6**, 680–690.

18 F. Gillot, J. Oró-Solé and M. R. Palacín, *J. Mater. Chem.*, 2011, **21**, 9997–10002.

19 P. Wang, J. Bai, K. Li, H. Ma, W. Li, X. Zhu, Y. Sun and B. Zhao, *Chem. Eng. J.*, 2021, **425**, 130607.

20 H. Zhou, Z. Li, K. Wang, M. Gao and S. Ding, *J. Mater. Chem. A*, 2019, **7**, 1779–1784.

21 C. Zhang, W. Hu, H. Jiang, J. K. Chang, M. Zheng, Q. H. Wu and Q. Dong, *Electrochim. Acta*, 2017, **246**, 528–535.

22 Y. Jin, C. Zhao, Z. Sun, Y. Lin, L. Chen, D. Wang and C. Shen, *RSC Adv.*, 2016, **6**, 30763–30768.

23 L. Shen, H. Song and C. Wang, *Electrochim. Acta*, 2017, **235**, 595–603.

24 L. Sun, J. Xie, Z. Chen, J. Wu and L. Li, *Dalt. Trans.*, 2018, **47**, 9989–9993.

25 Y. Ai, Z. Han, X. Jiang, H. Luo, J. Cui, Q. Bao, C. Jing, J. Fu, J. Cheng and S. Liu, *Small*, 2020, **16**, 2002701.

26 L. Gou, L. Ma, M. J. Zhao, P. G. Liu, X. D. Wang, X. Y. Fan and D. L. Li, *J. Mater. Sci.*, 2019, **54**, 1529–1538.

27 Y. G. Weng, Z. H. Ren, Z. R. Zhang, J. Shao, Q. Y. Zhu and J. Dai, *Inorg. Chem.*, 2021, **60**, 17074–17082.

28 C. Li, X. Lou, Q. Yang, Y. Zou and B. Hu, *Chem. Eng. J.*, 2017, **326**, 1000–1008.

29 H. Liu, H. Li, F. Cheng, W. Shi, J. Chen and P. Cheng, *Inorg. Chem.*, 2018, **57**, 10640–10648.

30 C. Shi, X. Wang, Y. Gao, H. Rong, Y. Song, H. J. Liu and Q. Liu, *J. Solid State Electrochem.*, 2017, **21**, 2415–2423.

31 A. Nazir, H. T. T. Le, A. G. Nguyen and C. J. Park, *Electrochim. Acta*, 2021, **389**, 138750.